Sulfamethoxazole Transformation by Heat-Activated Persulfate: Linking Transformation Products Patterns with Carbon and Nitrogen Isotope Fractionation

Xiao Liu[†,*], Jimmy Köpke [‡,§], Caglar Akay [‡,‖], Steffen Kümmel[#], Gwenaël Imfeld [†]

[†] Institut Terre et Environnement de Strasbourg (ITES), Université de Strasbourg/EOST/ENGEES, CNRS UMR 7063, F-67084 Strasbourg, France

[‡] Department of Molecular Environmental Biotechnology, Helmholtz Centre for Environmental Research-UFZ, Permoserstraße 15, 04318 Leipzig, Germany

[§] German Environment Agency, Section II 3.3, Schichauweg 58, 12307 Berlin, Germany

[‖] Department of Exposure Science, Helmholtz Centre for Environmental Research-UFZ, Permoserstraße 15, 04318 Leipzig, Germany

[#] Department of Technical Biogeochemistry, Helmholtz Centre for Environmental Research-UFZ, Permoserstraße 15, 04318 Leipzig, Germany

*Corresponding author: Xiao Liu (e-mail: xiaoliu@unistra.fr; imfeld@unistra.fr)

Manuscript for Environmental Science & Technology

ABSTRACT

Sulfamethoxazole (SMX) is a frequently detected antibiotic in groundwater, raising environmental concerns. Persulfate oxidation is used for micropollutant removal. To investigate SMX transformation by persulfate, experiments were conducted using heat-activated persulfate at pH 3, 7, and 10. TP269a (SMX hydroxylamine) and TP178 were identified as the dominant TPs across pH levels. The exclusive formation of 4-nitroso-SMX, 4-nitro-SMX, and TP518 at pH 3 highlighted the role of $SO_4^{\bullet-}$ in attacking the NH_2. At pH 7 and 10, 3A5MI emerged as the dominant TP. Carbon isotopic fractionation (ε_C = −1.3 ± 0.5‰, −1.1 ± 0.4‰, and −1.1 ± 0.3‰ at pH 3, 7 and 10) remained consistent across pH levels, caused by the formation of TP178 involving C-S bond cleavage. An inverse nitrogen isotope fractionation at pH 3 (ε_N = +0.68 ± 0.11‰) was associated with $SO_4^{\bullet-}$-induced single-electron transfer. Conversely, normal nitrogen isotope fractionation at pH 10 (ε_N = −0.27 ± 0.04‰) was associated with N-H bond cleavage by H abstraction through HO• and N-S bond cleavage. The inverse nitrogen isotope fractionation at pH 7 indicated that the dominant pathway involved $SO_4^{\bullet-}$ reactions, accounting for 74%. Overall, the results highlight the potential of CSIA to elucidate SMX persulfate oxidation pathways.

Key words: micropollutant, heat-activated persulfate, isotope fractionation, radical reactions

Synopsis: This study highlights the potential of compound-specific isotope analysis of sulfamethoxazole and serves as a refence in characterizing its radical reactions, with implications for assessing transformation in aquatic ecosystems.

INTRODUCTION

The increasing prevalence of pharmaceutical residues in aquatic systems presents significant environmental and public health challenges. Sulfamethoxazole (SMX), a widely used sulfonamide antibiotic, is particularly concerning due to its extensive application in both human and veterinary medicine.[1,2] This widespread use has led to persistence of SMX in various aquatic ecosystems, primarily through effluent from wastewater treatment plants, agricultural runoff, and improper disposal of pharmaceutical products. [3,4] The recalcitrant nature of SMX poses risks, such as the promotion of antibiotic-resistant bacteria and disruption of aquatic ecosystems,[5] which counteracts with the concept of One Health.[6] Addressing these risks requires a comprehensive understanding of SMX environmental behavior and its transformation mechanisms to develop effective removal strategies.

In recent years, *in situ* chemical oxidation (ISCO) has emerged as a promising technology for remediating organic contaminants in environmental systems. Among ISCO methods, activated persulfate (PS) oxidation has gained considerable attention for its effectiveness in degrading pollutants in contaminated groundwater and soil.[7–9] This process relies on the formation of highly reactive sulfate radicals ($SO_4^{\bullet-}$, E_0 = 2.5-3.1 V, depending on pH) through the activation of sodium persulfate (PS) by heat, transition metals, UV light, or base.[10,11] The generation of reactive species from PS is pH-dependent, as the pH value influences both the formation of $SO_4^{\bullet-}$ and the speciation of organic compounds with ionizable functional groups. At basic pH values, $SO_4^{\bullet-}$ can convert into hydroxyl radicals (HO•).[12]

Traditionally, identifying specific transformation products (TPs) has been fundamental to elucidating the degradation pathways of organic pollutants. However, TP often fail to differentiate among radical-induced degradation mechanisms, as similar TPs—such as hydroxylated SMX derivatives or dimers[9,13] —can result from different reactive species,

including HO• and $SO_4^{\bullet-}$. This limitation poses a challenge in understanding the distinct degradation pathways and mechanisms driven by these radicals, thereby hindering efforts to guide remediation strategies and assess environmental risks. Consequently, developing effective approaches to distinguish among SMX radical reactions has become a pressing priority.

Advanced analytical techniques, such as gas chromatography-mass spectrometry (GC-MS) and liquid chromatography-mass spectrometry (LC-MS), have been widely used to investigate the degradation mechanisms of organic pollutants. However, these methods often depend on the chemical fingerprint of degradation products, which can be ambiguous or inconclusive due to overlapping reaction mechanisms. This uncertainty complicates result interpretation and restricts deeper investigations into the environmental behavior of organic pollutants.

To address these limitations, multi-element compound-specific isotope analysis (ME-CSIA) has emerged as a powerful tool for characterizing and differentiating pollutant degradation processes. [14–16] ME-CSIA measures the stable isotope ratios of specific elements within a compound, providing high reliability and accuracy as it remains unaffected by other reactants, products, or elements. Typically, normal isotope fractionation occurs when lighter isotopes, such as ^{12}C, involved in bond cleavage, react more quickly than their heavier counterparts, like ^{13}C, leading to an increase in $^{13}C/^{12}C$ ratios in the remaining parent compound. Conversely, an inverse isotope effect results in a decrease in the $^{13}C/^{12}C$ ratios. Single-element isotope analysis (e.g., ^{13}C-CSIA) has been used to characterize the direct photolysis of SMX, its indirect photolysis mediated by oxidants such as O_3 and ClO_2,[17] and its aerobic degradation by *Microbacterium* sp. strain BR1,[18] as well as anaerobic degradation by *Desulfovibrio vulgaris* Hildenborough.[19] Recent advancements include the development of ^{15}N- and $^{33/34}S$-CSIA for SMX using gas chromatography-isotope ratio mass spectrometer (GC-IRMS) and gas

chromatography–multi collector–inductively coupled plasma mass spectrometry (GC-MC-ICPMS), respectively.[20,21] ME-CSIA has also been successfully applied to characterize and distinguish the direct photolysis of SMX, demonstrating pH-dependent processes.[19] In the context of PS oxidation of SMX, only carbon and nitrogen isotope analyses were performed. High sulfur content from PS addition interfered with sulfur isotope measurements by disrupting the background signal and resolution. Additionally, insufficient SMX concentration, even after enrichment efforts, prevented hydrogen isotope analysis. Beyond single-element isotopic fractionation, dual-element isotope analysis has been successfully applied to study the degradation processes of emerging contaminants, such as diclofenac[22] and ibuprofen.[23]

We hypothesized that the SMX transformation by HO• and $SO_4^{\bullet-}$ induces distinct reaction mechanisms, leading to specific SMX TPs and unique isotope fractionation patterns. To test this hypothesis, we established reference radical reaction systems, including heat-activated persulfate, to examine the reactions of HO• and $SO_4^{\bullet-}$ at pH 3, 7 and 10. We investigated potential degradation pathways and mechanisms, such as single electron transfer, hydrogen abstraction, and multi-bond cleavages, by integrating data on reaction kinetics, transformation products (TPs), carbon and nitrogen stable isotope ratios and apparent kinetic isotope effect (AKIE) values.

METHODS AND MATERIALS

Details of chemicals are listed in Section 1 (S1) of the Supporting Information (SI).

Heat-activated persulfate transformation experiments. Heat-activated persulfate experiments were conducted with SMX in a 10 mM phosphate buffer at pH 3 and pH 7, and in a 10 mM carbonate buffer at pH 10. Persulfate oxidation was initiated at an activation temperature of 40 °C. The initial SMX concentration was approximately 900 μM, with a 25:1 molar ratio of persulfate to SMX. The reaction was carried out in a glass bottle covered with

aluminum foil, with a starting volume of 200 mL, in an incubator set to 40 °C and shaken at 200 rpm. At various time intervals, 200 μL aliquots were taken for concentration and transformation product analysis. To quench the reactions, an equal volume (200 μL) of methanol (MeOH) was immediately added to each sample, which were then stored at 4 °C until analysis. Additionally, aliquots ranging from 5 to 50 mL were collected for CSIA measurement. Prior to CSIA, all samples were cleaned up using solid-phase extraction (SPE) immediately after sampling to prevent further reactions. Control experiments were conducted under the same conditions but without addition of persulfate.

Sample preparation by solid-phase extraction. We used Oasis HLB cartridges (6 mL cartridges, 200 mg; Waters, Milford, MA, USA) for sample clean-up. The cartridges were preconditioned with 5 mL of acetonitrile, followed by 5 mL of ethyl acetate, and finally with 5 mL of Milli-Q water. Samples were then percolated through the cartridges drop by drop under vacuum and subsequently dried under vacuum for 30 minutes. SMX was eluted with 5 mL of ethyl acetate and 5 mL of acetonitrile. The eluent was dried under a gentle nitrogen stream, resuspended in 1 mL of acetone, and stored at 4 °C until analysis. The recovery rate was 93 ± 2%, and the stable isotopic compositions of SMX were not significantly altered by the extraction procedure (Δ < 1‰), as previously reported.[19]

Analytical Methods. *Concentration Analysis.* SMX concentrations were monitored using Ultra-Performance Liquid Chromatography with Diode Array Detection (UPLC-DAD) system (Thermo Fischer UltiMate 3000 RS Diode Array Detector, Germany),[24] as detailed in S2 (SI).

Transformation Product (TP) Analysis. Transformation products were analyzed using an Agilent 1260 Infinity II Series liquid chromatography (LC) system coupled to an AB Sciex QTRAP 6500+ tandem mass spectrometer (MS/MS) equipped with a Turbo V ion source, following a previously described protocol.[19] Electrospray ionization was performed in both

positive and negative polarity modes. Chromatographic separation was achieved using an Agilent Zorbax Eclipse Plus Rapid Resolution HT-C18 column (100 mm x 3.0 mm, 1.8 µm) coupled to a Phenomenex Security guard cartridge system (C18; ODS, Octadecyl) as a guard-column. Other details can be found in S2 (SI).

Carbon and Nitrogen Isotope Analysis. Carbon and nitrogen isotopic compositions ($\delta^{13}C$ and $\delta^{15}N$) were determined using a gas chromatograph−isotope ratio mass spectrometer (GC-IRMS). The gas chromatograph (Trace 1310, Thermo Fisher Scientific, Germany) was connected to a MAT 253 IRMS system (Thermo Fisher Scientific, Germany) through a GC-IsoLink and a ConFloIV interface (Thermo Fisher Scientific, Germany). Chromatographic separation was achieved using a Zebron ZB1 column (60 m × 0.32 mm × 1 µm; Phenomenex, Germany) with a constant carrier gas flow of 2 mL min^{-1} was applied for chromatographic separation. Each sample aliquot (1-5 µL) was injected via an autosampler (TriPlus RSH, Thermo Fisher Scientific, Germany) in split mode, with a split ratio of 1:3 at 200 °C. The oven temperature was initially held at 40 °C for 5 min, then increased at 10 °C min^{-1} to 300 °C, where it was held for 15 min.

For carbon isotope analysis, SMX was converted to CO_2 at 1,000 °C in a combustion oven (Thermo Fisher Scientific, Germany). For nitrogen isotope analysis, SMX was derivatized using trimethylsilyldiazomethane (TMSD), methylating the nitrogen atom within the S-N bond. The nitrogen isotopic composition of the SMX derivative remained constant after derivatization, showing a systematic offset of 1.5‰ compared to the non-derivatized SMX analyzed via EA-IRMS.[19] The SMX derivative was then converted to NO_x at 1000 °C in a combustion oven (Thermo Fisher Scientific, Germany) and further reduced to N_2 in a custom-made reduction oven. This oven comprised a tubular ceramic tube (320 mm length, 0.8 mm inner diameter, 1.6 mm outer diameter; Degussit AL23 aluminum oxide ceramic, Friatec, Germany) filled with three copper wires (300 mm length, 0.125 mm diameter; Goodfellow, Germany) maintained at

600 °C. Triplicate measurements demonstrated reproducibility consistently within the total error for $\delta^{13}C$ (0.5‰) and $\delta^{15}N$ (0.5‰), encompassing both accuracy and reproducibility.

Data Analysis. First-order kinetic constants (*k*) were determined by fitting a first-order kinetic model to the concentration data. The isotopic fractionation of a specific element (ε_E) was calculated by the slope of the linear regression through the plot of $\ln(C_t/C_0)$ versus $\ln[(\delta_t + 1)/(\delta_0 + 1)]$, in accordance with the Rayleigh equation (Eq. 1). Here, δ represents the isotopic composition of an element, C_t/C_0 denotes the residual fraction of the substrate, and *t* refers to the sampling time, with 0 indicating the initial time before the reaction begins. The error associated with ε_E was reported as 95% confidence interval (CI), determined through regression curve analysis.

$$\ln\left(\frac{\delta_t+1}{\delta_0+1}\right) = \varepsilon_E \times ln\frac{C_t}{C_0} \quad (1)$$

The dual isotope ($\Lambda_{E1/E2}$) values for element 1 (E_1) and 2 (E_2) were calculated from the slope of the fitted line obtained by plotting ΔE_1 values against ΔE_2 values.[15] Here, Δ represents the change in isotopic composition between the samples and their initial values. The 95% confidence level of the slope was also determined.

An extended Rayleigh-type equation (Eq. 2) was derived to quantify the contribution of two simultaneous transformation processes that affect the same substrate via distinct mechanisms.[25] In this equation, *F (%)* represents the contribution of the first process to the overall reaction, considering two competing degradation pathways. The terms ε_A, ε_1 and ε_2 correspond to the kinetic isotopic fractionation of the overall reaction (A), and the individual process 1 and 2, respectively. The 95% confidence interval for *F* was calculated using error propagation.

$$F = \frac{\varepsilon_A-\varepsilon_2}{\varepsilon_1-\varepsilon_2} \quad (2)$$

The dual isotope slope (Λ) values were determined using ordinary linear regression. The symbol Δ represents the deviation of isotopic composition from the initial values of the samples. For example, $\Lambda_{N/C}$ values were calculated as the slope of the fitted line obtained by plotting $\Delta^{15}N$ values against $\Delta^{13}C$ values. Furthermore, the 95% confidence interval for the slope was calculated to determine the uncertainty associated with Λ values

According to Elsner et al.,[26] Eq. 3 was applied to calculate the apparent kinetic isotope effect (AKIE) for SMX.

$$\text{AKIE}=\frac{1}{1+z\times\varepsilon_{bulk}\times\frac{n}{x}/1000} \quad (3)$$

where n is the number of atoms of the element, x the number of atoms at reactive sites, and z the number of indistinguishable reactive positions for intramolecular competition.

RESULTS AND DISCUSSION

SMX Transformation Kinetics. The transformation kinetics of SMX in persulfate (PS) systems varied across different pH levels, with the highest rate at pH 7. The transformation rate of SMX in PS systems is primarily affected by two pH-dependent factors: (i) the speciation of SMX and (ii) the formation of dominant radicals with varying reactivity. Within the studied pH range, SMX (pKa_1=1.6 ± 0.2 and pKa_2=5.7 ± 0.2)[27] exists in neutral forms at pH 3 and as an anion at pH 7 and pH 10 (Figure S1, SI). A radical scavenger experiment was conducted using ethanol (EtOH) and tert-butanol (TBA) to identify the predominant reactive radicals at different pH levels. EtOH effectively quenched both $SO_4^{\bullet-}$ and HO•, with second-order rate constants ranging from 1.2 – 2.8 × 10^9 M^{-1} s^{-1} for the EtOH/ HO• system and 1.6 – 7.7 × 10^7 M^{-1} s^{-1} for the EtOH/$SO_4^{\bullet-}$ system.[9] In contrast, TBA is widely recognized as a selective scavenger for HO• due to its low reactivity with $SO_4^{\bullet-}$ (k = 4 – 9.1 × 10^5 M^{-1} s^{-1}) compared to its high reactivity with HO• (k = 3.8 – 7.6 × 10^8 M^{-1} s^{-1}).[9] As shown in Figure S2, the addition of EtOH and TBA

inhibited SMX transformation, with the extent of inhibition varying across pH levels. At pH 3, the degradation rate was significantly slower in the presence of EtOH (kinetic value: –0.0129 ± 0.0041) compared to TBA (kinetic value: –0.0653 ± 0.0026), suggesting that SO4•– is the predominant radical under acidic conditions. At pH 7, kinetics for EtOH (–0.1130 ± 0.0051) and TBA (–0.1501 ± 0.0063) indicated that both SO4•– and HO• coexisted and contributed to the SMX degradation. Under alkaline conditions (pH 10), the reaction rates for EtOH (–0.1690 ± 0.0129) and TBA (–0.1721 ± 0.0036) were similar, indicating that HO• was the dominant radical species. The findings are consistent with previous studies. [7,9,12,28,29]

Phosphate and carbonate buffers (10 mM) were used to stabilize pH levels. However, reactions between $SO_4^{\bullet-}$ and HO• with buffer ions can generate secondary radicals, such as $HPO_4^{\bullet-}$, $H_2PO_4^{\bullet-}$, $CO_3^{\bullet-}$, and $HCO_3^{\bullet-}$, potentially influencing SMX transformation. According to the literature,[30–33] the reaction rate constants of $SO_4^{\bullet-}$ and HO• with the buffer ions were at least three magnitudes lower compared to their rate constants with SMX, except for the reaction between HO• and $CO_3^{\bullet-}$, which was only one order of magnitude lower (Table S1, SI). Additionally, the buffer concentration used in this study (10 mM) was significantly lower than in other studies.[13,34] Consequently, no phosphorus and carbonate-related TPs were detected (see section on TPs below). Thus, the contribution of secondary radicals during PS transformation was considered negligible and was not included in estimating the contributions of $SO_4^{\bullet-}$ and HO• to SMX transformation.

Interestingly, OH• exhibited similar reactivity with both the neutral and anionic form of SMX, whereas $SO_4^{\bullet-}$ showed higher reactivity with the SMX anion compared to the neutral form. This increased reactivity is attributed to the enhanced electron-donating effect of SMX through sulfonamide nitrogen deprotonation, which favors an electrophilic attack by $SO_4^{\bullet-}$.[13] The second-order rate constants for the reaction of SMX with $SO_4^{\bullet-}$ were approximately (9.6 ± 1.5) × 10^8 $M^{-1}s^{-1}$ at pH 3 and (1.34 ± 0.02) × 10^{10} $M^{-1}s^{-1}$ at pH 7.[13] In comparison, the second-

order rate constants for the reaction of SMX with HO• were (7.6 ± 0.9) × 10^9 $M^{-1}s^{-1}$ across all pH values.[13]

The significantly higher kinetic values at pH 7 than at pH 3 suggest that the SMX anion is more reactive with $SO4^{\bullet-}$ than the neutral form, consistent with previous studies.[9,12,13] The slightly higher transformation rate of SMX at pH 7 than at pH 10 was attributed to the predominance of $SO_4^{\bullet-}$ at pH 7, whereas HO• radicals dominate at pH 10.

Identification of SMX Transformation Products. TPs of SMX in persulfate transformation were identified based on their *m/z* ratios in neutral mass and are listed in Tables S2-S4 (SI). TP98 (3-amino-5-methyl isoxazole, 3A5MI) was confirmed using an authentic standard. However, analytical standards for most TPs are not commercially available. To enable comparison of TPs across pH values, the corresponding peak areas were presented as peak area ratios (PAR), defined as the ratio of each TP's peak area to the initial SMX peak area before irradiation. Peak normalization was used to track changes in other TPs during transformation. This was done by calculating the ratio of each TP's peak area at a specific time point to its maximum peak area observed across all time points, as shown in Figures S3–S5. All TPs identified at pH 3, pH 7, and pH 10 are presented in Schemes 1, 2, and 3, respectively.

pH3. At pH 3, the aniline moiety of SMX was the preferred reactive site for $SO_4^{\bullet-}$ due to its high electrophilicity. The interaction between $SO_4^{\bullet-}$ and the aniline moiety produced a radical cation (SMX^+) through a single-electron transfer mechanism.[31,35,36] This SMX^+ is unstable and undergoes hydrolysis, yielding OH-SMX. Given the electron-donating effect of the NH_2 group and the electron-withdrawing effect of the SO_2-NH group, mono-hydroxylation of SMX likely occurred at the ortho position, forming TP269b, consistent with previous studies.[9]

Alternatively, SMX^+ can undergo deprotonation to generate an anilinyl radical, which is further oxidized by $SO_4^{\bullet-}$ to form hydroxylamine (TP269a). TP269a then further oxidized to 4-nitroso-SMX (TP267) and subsequently 4-nitro-SMX (TP283).[9,12] Further hydroxylation of nitroso- and nitro-SMX by $SO_4^{\bullet-}$ can produce TP299a and TP299b. Concurrently, coupling of the *N*-centered radical can generate TP502,[9,13] undergoing further oxidation to generate TP518 (Scheme S1). TP267, TP283, and TP518 are detected only at pH 3, indicating efficient $SO_4^{\bullet-}$ attack on the NH_2 group and subsequent oxidation of TP502.

TP98 (3A5MI) and TP178 are formed by the cleavage of S-N and S-C bonds in SMX by $SO_4^{\bullet-}$, which is commonly observed in SMX oxidation by advanced oxidation processes.[37,38] Additionally, TP239 results from the deamination of SMX, TP270 is likely produced through NH_2 substitution of TP269a by OH, and TP112 is formed by further oxidation of 3A5MI. These TPs were reported previously during SMX oxidation via radical reactions.[17,39,40] Notably, high-molecular mass TPs (>300), such as TP365 and TP379, were first observed during SMX oxidation by PS. *N*-centered radicals from hydroxylated SMX (TP269a) and 3A5MI likely responsible for the formation of TP365 and TP379b. The detection of these TPs during PS oxidation may be related to the high SMX concentrations used in this study, enabling the detection of minor TPs. Based on the PAR value, dominant TPs include TP178 and TP269a as primary TPs, with TP267, TP283, TP379b, and TP518 as secondary TPs (Figure 1).

For TP269, two isomers were identified with characteristic fragments at 108, 124, and 172, suggesting hydroxylation on the aniline moiety, either the aromatic ring or the amino group. However, distinguishing whether oxygen was added to the aromatic ring or if a hydroxylamine was formed is challenging based on these fragments alone. Since the NH_2 group is the preferred reactive site for $SO_4^{\bullet-}$, it is reasonable to hypothesize that the dominant TP269a is hydroxylamine, while TP269b likely results from hydroxylation of the aromatic ring. The

variation in nitrogen isotope patterns at different pH values, particularly the inverse nitrogen isotope fractionation at pH 7, further supports this hypothesis (see detailed discussion below).

pH10. At pH 10, HO• is the predominant radical species, leading to a different pattern of TPs than at pH 3. The primary dominant TPs at pH 10 were 3A5MI, TP178 and TP269a (Figure 1). When HO• reacts with aniline, hydrogen abstraction is the preferred pathway, contrasting with the single-electron transfer mechanism induced by $SO_4^{\bullet-}$. HO• is expected to attack aniline at various positions. Previous studies have shown that the hydrolysis of aniline radicals formed by HO• attack through hydrogen abstraction produces hydroxylated radical products, which further react with O_2 to form hydroxylated anilines.[41] This explains the formation of TP269a and TP269b through reaction at the NH_2 and ortho-position of aniline (Scheme S2). Previous study [17] found that the hydroxylamine was dominantly formed during SMX transformation by HO• from ozone and chlorine dioxide which is consistent with our study. TP502 is formed through the coupling of aniline radicals derived from the NH_2 group by H abstraction (Scheme S2), as shown in previous studies of SMX transformation in UV/H_2O_2 system.[13]

The different patterns of TPs between reactions of SMX with HO• and $SO_4^{\bullet-}$ were mainly attributed to the reactivity of these radicals to specific groups of SMX. For instance, $SO_4^{\bullet-}$ more efficiently attacked the NH_2 group, favoring the formation of nitrogen-oxidized products. This idea is supported by the formation of TP267 and TP283 at pH3, while these TPs were not detected at pH 10. 3A5MI and TP178 were formed by the bond cleavage similar to that observed at pH 3. Several minor TPs, including TP112, TP239 and TP379, were also observed, as seen at pH 3. TP347 can be explained as the coupling of *N*-centered radicals at the amino group of 3A5MI and SMX, a phenomenon first observed during PS oxidation and in cobalt/peracetic acid transformation of SMX.[42]

pH7. At pH 7, both HO• and SO4•– radicals contributed to the reactions. The primary dominant TPs were 3A5MI, TP178 and TP269a (Figure 1). Other minor TPs were similar to those discussed previously. Although the TP pattern at pH 7 more closely resembled to that at pH 10, identifying the dominant underlying transformation mechanism at pH 7 was not possible, as most TPs were similar across all pH values.

Overall, distinguishing the underlying processes of HO• and $SO4^{\bullet-}$ radical reactions solely based on TP formation is challenging. This complexity motivated us to conduct CSIA to examine whether stable isotope fractionation can differentiate radical reactions, even when similar TPs are present. Additionally, we aimed to determine whether the isotope signature of SMX radical reactions can be differentiated from other processes, such as phototransformation and microbial transformation.

Stable Isotope Fractionation of SMX. The heat-activated PS transformation of SMX involves multi-element reactions. Integrating multi-element stable isotope fractionation data can characterize transformation mechanisms and reveal distinct isotope patterns in SMX transformation. In all control experiments without PS, SMX concentrations and isotopic composition remained unchanged, confirming that SMX was only transformed with PS (Table S5 and Figure S6, SI).

Carbon isotope fractionation. During SMX transformation in PS systems, normal and consistent carbon isotope fractionation values were observed across pH values. Differences in carbon isotopic compositions ($\Delta\delta^{13}C$) of SMX between samples and initial values were 2.2‰ at pH 3 for 76% transformation, 2.3‰ at pH 7 for 88% transformation, and 1.9‰ at pH 10 for 83% transformation, respectively (Figure 2). This suggests that carbon bond cleavage was involved in the first irreversible rate-limiting step of SMX transformation. The Rayleigh plots with regressions were shown in Figure S7 and carbon isotopic fractionation (ε_C) showed no significant differences across pH values (−1.3 ± 0.5‰ at pH 3, −1.1 ± 0.4‰ at pH 7, and −1.1

± 0.3‰ at pH 10; Table 1), indicating a similar transformation mechanism involving carbon bond cleavage mediated by $SO_4^{\bullet-}$ and HO•.

Based on the TP patterns, carbon isotopic fractionation was mainly attributed to a kinetic isotope effect involving C-S bond cleavage, resulting in the formation of TP178, which dominated across pH values. This explains the consistent ε_C values across pH values. Since the reaction systems involves multi bond cleavages, the nitrogen isotope fractionation was also caused by a primary isotope effect. The ε_C values for SMX direct phototransformation (−2.0 ± 0.2‰ at pH 7 and −2.8 ± 0.4‰ at pH 3),[20] aerobic (−0.6 ± 0.1‰),[18] and anaerobic biotransformation (−5.7 ± 0.8‰)[19] differed significantly from those observed in this study (Table 1). This suggests distinct mechanism of SMX transformation involving carbon bond cleavage in the rate-limiting step. Based on the formation of TPs, SMX primarily undergoes C-S bond cleavage when exposed to heat-activated PS. In contrast, carbon isotope fractionation during direct phototransformation of SMX at pH 7 resulted from multiple carbon bond cleavages, whereas at pH 3, it was caused by isomerization involving a C=C bond cleavage.[20] However, in the aerobic biotransformation of SMX by *Microbacterium* sp. strain BR1, the *ipso*-hydroxylation acts as the rate-limiting step, leading to less pronounced carbon isotope fractionation,[18] while in the anaerobic biotransformation by *Desulfovibrio vulgaris*, isomerization involving a C=C bond cleavage is the key step,[19] creating stronger carbon isotope fractionation than those observed in our study. In contrast, ε_C values for O_3 and ClO_2 oxidation were similar to those in the current study. This similarity can be attributed to carbon isotope fractionation occurring through the attack on aromatic carbon bonds, leading to the formation of TP178, as observed in the heat-activated PS systems.[17]

The ^{13}C-AKIE values resulting from the C –S bond cleavage were consistent across pH values, ranging from 1.011 ± 0.004 to 1.013 ± 0.005. These values fall within the typical range for an S_N1 reaction (1.01-1.03), [26] suggesting that the C –S bond cleavage may proceed via an

362 S_N1 reaction. However, specific ^{13}C-AKIE values for S_N1 reactions involving C –S bonds are
363 not available for direct comparison.

364 *Nitrogen isotope fractionation.* An inverse nitrogen isotope fractionation was observed
365 during SMX transformation by PS at pH 3 and pH 7 (ε_N = +0.7 ± 0.1‰ at pH 3 and +0.4 ± 0.2‰
366 at pH 7) (Figure 2). The absence of significant difference in ε_N between these pH values
367 suggests that a similar nitrogen bond cleavage dominated SMX transformation at both pH
368 values. In contrast, normal nitrogen isotope fractionation was observed at pH 10 (ε_N = −0.3 ±
369 0.04‰), indicating a different transformation mechanism compared to the other pH values.

370 Inverse nitrogen isotope fractionation has been reported in various transformation
371 processes of nitrogen-containing pollutants, such as the direct phototransfromation of atrazine[43],
372 diclofenac[22] and chloroanilines,[44,45] as well as SMX[20] and oxidation of substituted anilines.[46]
373 The inverse nitrogen isotope fractionation observed during SMX transformation by PS at pH 3
374 could primarily be attributed to the single-electron transfer mechanism induced by $SO_4^{\bullet-}$, as
375 supported by the formation of TP269a, TP267, TP283, TP502, and TP518. We hypothesize that
376 this process involves the formation of a *N*-centered radical intermediate, which delocalizes over
377 the aromatic ring, forming partial imine-type bonding of nitrogen in subsequent intermediates.[46]
378 Consequently, the C-N bond becomes less prone to a cleavage in the transition state. This is
379 further supported by the higher infrared stretching frequencies of C=N compared to C-N bonds,
380 indicating stronger nitrogen bonds in imines.[46] Similarly, inverse nitrogen isotope fractionation
381 was reported in single-electron transfer mechanisms during oxidation of substituted anilines by
382 MnO_2.[46]

383 In contrast, the normal nitrogen isotope fractionation during SMX transformation
384 induced by HO• at pH 10 was primarily due to hydrogen abstraction from the amino group,

forming an aminyl radical, which leads to N-H bond cleavage forming TP269a and N-S bond cleavage resulting in the formation of 3A5MI (Scheme S2).

A lower inverse nitrogen isotope fractionation was observed at pH 7 compared to pH 3. The nitrogen isotope fractionation at pH 7 was primarily driven by the formation of 3A5MI and TP269a. 3A5MI is formed by N-S bond cleavage, which induces normal nitrogen isotope fractionation. However, TP269a may be formed through two mechanisms: single electron transfer or hydrogen abstraction, leading to divergent nitrogen isotope fractionation patterns. Therefore, the inverse nitrogen isotope fractionation observed at pH 7 likely resulted from a combined effect of reactions involving $SO_4^{\bullet-}$ and HO•. This observation also suggests that SMX hydroxylamine was likely the dominant TP269 species. If dominant hydroxylation had occurred on the aromatic rings, it would have resulted in normal carbon isotope fractionation at pH 7, and the nitrogen isotope fractionation at pH 7 would have been solely due to 3A5MI, typically leading to normal nitrogen isotope fractionation.

Additionally, the protonation/deprotonation equilibrium of SMX at pH 7 and pH 10 could influence the isotopic composition of the nitrogen atom linked to the hydrogen, potentially altering its electronic structure. Assuming that only the neutral form of SMX is reactive, nitrogen isotope fractionation at these pH values may result from protonation of the SMX anion to the neutral form, followed by subsequent radical reactions. The distinct nitrogen isotope fractionation ─inverse at pH 7 and normal at pH 10 ─ suggests that protonation of the SMX anion is not the primary factor driving the observed isotope fractionation. Instead, radical reactions are the main factor affecting nitrogen isotope fractionation. Therefore, ε_N values can be used to estimate the contribution of $SO4^{\bullet-}$ and HO• related reactions to the overall transformation reaction.

The Rayleigh equation modified by Van Breukelen (2007) [25] was used to estimate the contribution of two co-occuring pathways to the overall SMX transformation (see S11 in the SI). At pH 7, analysis of the ε_N values indicated that 74 ± 16% of the SMX transformation was attributed to $SO_4^{\bullet-}$, while 26 ± 16% was attributed to HO• (see S9, SI). This indicates that SMX is preferentially transformed through reaction with $SO_4^{\bullet-}$ in the PS system at pH7, providing additional insights beyond TP patterns alone.

Currently, nitrogen isotopic fractionation during SMX transformation has only been reported for direct phototransformation (ε_N = +3.6 ± 0.1‰ at pH 3 and +3.0 ± 0.2‰ at pH 7)[20] with ε_N values significantly different from those reported in this study. Our results indicate that despite the formation of similar TPs, such as hydroxylated TPs which were observed across all experiments as well as in direct phototransformation experiments, nitrogen isotopic fractionation facilitates differentiation among distinct reaction mechanisms. Specifically, inverse nitrogen isotopic fractionation induced by single-electron transfer mechanisms via radical reactions can be distinguished from that induced by singlet and triplet photoreactions. Conversely, normal nitrogen isotopic fractionation caused by H abstraction or N-S bond cleavage by HO• could also be distinguished.

Nitrogen isotope fractionation at pH 7 and pH 10 was affected by multiple mechanisms and bond cleavages, making it challenging to directly calculate ^{15}N-AKIE values for these conditions. At pH 3, the ^{15}N-AKIE values (0.998 ± 0.001) falls within the range observed for the oxidation of 3-chloroaniline (^{15}N-AKIE = 0.9985 ± 0.0002),[46] which was also induced by a single-electron transfer. This finding further supports the hypothesis that nitrogen isotope fractionation at pH 3 is driven by single-electron transfer.

Dual element isotope analysis. In this study, nitrogen isotope fractionation at pH 7 and pH 10 was affected by various mechanisms and bond cleavages, which limits the use of ME-CSIA. Therefore, caution is necessary when using the dual-element isotope approach to identify

transformation mechanisms in systems where multiple bond cleavages occur.[20] The $\Lambda_{N/C}$ values at pH 7 and pH 3 are similar, indicating that the primary transformation mechanism of SMX was consistent at these pH values. In contrast, a distinct $\Lambda_{N/C}$ value was observed at pH 10, suggesting a different degradation pathway under alkaline conditions. These findings align with the conclusions drawn from single-element isotope analysis. Additionally, dual-element isotope analysis demonstrated greater effectiveness than single-element CSIA in identifying and distinguishing transformation mechanisms, particularly in field studies. The $\Lambda_{N/C}$ values observed in direct phototransformation differ significantly from those observed during PS oxidation, further confirming the involvement of distinct transformation processes.

ENVIRONMENTAL IMPLICATIONS

In this study, we examined the potential and added value of multi-element compound-specific isotope analysis as a complementarily tool to TP analysis for monitoring the radical oxidation of the widely used antibiotic SMX. Additionally, we aimed to differentiate radical oxidation from other transformation processes in the environment. Our findings highlight distinct isotope patterns associated with SMX radical oxidation, induced by different radical reactions. Specifically, the stable isotope pattern of normal carbon and nitrogen isotope fractionation induced by HO•, as well as normal carbon and inverse nitrogen fractionation induced by $SO_4^{\bullet-}$, can be used to differentiate these radical reactions from other transformation processes occurring under natural conditions, such as direct phototransformation and biotransformation.

Radical oxidation processes are extensively used in wastewater treatment plants to improve the quality of receiving waters. Understanding the degradation of SMX by different radicals across varying pH values is critical for optimizing PS oxidation processes to maximize contaminant removal. Moreover, elucidating degradation pathways and identifying

intermediate products are essential to minimize the formation of potentially harmful or persistent by-products.

The isotope signatures derived from the current mechanistic studies provide valuable insights into predicting SMX behavior and degradation efficiency in both natural and engineered aquatic systems. Additionally, the application of ME-CSIA is a powerful tool for tracing SMX degradation mechanisms, confirming radical involvement, and quantifying the extent of SMX degradation in complex environmental systems.

AUTHOR INFORMATION

Corresponding Authors

*Xiao Liu: email: xiaoliu@unistra.fr; imfeld@unistra.fr

ORCID

Xiao Liu: 0000-0002-5363-6331

Jimmy Köpke: 0009-0009-4193-2764

Caglar Akay: 0000-0002-3371-5235

Steffen Kümmel: 0000-0002-8114-8116

Gwenaël Imfeld: 0000-0002-7054-4666

Author Contributions

The manuscript was written through contributions of all authors. All authors have given approval to the final version of the manuscript.

Notes

All authors of the article disclose no actual or potential conflict of interest including any financial, personal or other relationships with other people or organizations within three years of beginning the submitted work that could inappropriately influence, or be perceived to influence, their work.

Supporting Information

Information on chemicals, proportion of SMX species at different pH levels, analytical methods, list of potential transformation products, time trend of changes of peak area of TPs, proposed main transformation pathways, concentration and isotopic compositions of SMX in control experiments, and estimation of the relative contributions of $SO_4^{\bullet-}$ and HO• at pH 7.

ACKNOWLEDGEMENTS

X. Liu was supported by a Marie-Curie Postdoctoral fellowship funded by the European Commission, Grant number 101108336. We express gratitude for the use of the analytical facilities at the Laboratories for Stable Isotopes (LSI) and the Centre for Chemical Microscopy (ProVIS) at Helmholtz Centre for Environmental Research - UFZ, Leipzig. We thank Stefan Trapp (Technical University of Denmark) for helpful discussion and calculation of proportion of SMX species at different pH values.

REFERENCES

(1) Yang, Y.; Zhang, X.; Jiang, J.; Han, J.; Li, W.; Li, X.; Yee Leung, K. M.; Snyder, S. A.; Alvarez, P. J. J. Which Micropollutants in Water Environments Deserve More Attention Globally? *Environ Sci Technol* **2022**, *56* (1), 13–29. https://doi.org/10.1021/acs.est.1c04250.

(2) Luo, Y.; Guo, W.; Ngo, H. H.; Nghiem, L. D.; Hai, F. I.; Zhang, J.; Liang, S.; Wang, X. C. A Review on the Occurrence of Micropollutants in the Aquatic Environment and Their Fate and Removal during Wastewater Treatment. *Sci Total Environ* **2014**, *473–474*, 619–641. https://doi.org/10.1016/j.scitotenv.2013.12.065.

(3) Akay, C.; Ulrich, N.; Rocha, U.; Ding, C.; Adrian, L. Sequential Anaerobic-Aerobic Treatment Enhances Sulfamethoxazole Removal: From Batch Cultures to Observations

in a Large-Scale Wastewater Treatment Plant. *Environ Sci Technol* **2024**, *58* (28), 12609–12620. https://doi.org/10.1021/acs.est.4c00368.

(4) Achermann, S.; Bianco, V.; Mansfeldt, C. B.; Vogler, B.; Kolvenbach, B. A.; Corvini, P. F. X.; Fenner, K. Biotransformation of Sulfonamide Antibiotics in Activated Sludge: The Formation of Pterin-Conjugates Leads to Sustained Risk. *Environ Sci Technol* **2018**, *52* (11), 6265–6274. https://doi.org/10.1021/acs.est.7b06716.

(5) Yan, R.; Wang, Y.; Li, J.; Wang, X.; Wang, Y. Determination of the Lower Limits of Antibiotic Biodegradation and the Fate of Antibiotic Resistant Genes in Activated Sludge: Both Nitrifying Bacteria and Heterotrophic Bacteria Matter. *J Hazard Mater* **2022**, *425*. https://doi.org/10.1016/j.jhazmat.2021.127764.

(6) Hernando-Amado, S.; Coque, T. M.; Baquero, F.; Martínez, J. L. Defining and Combating Antibiotic Resistance from One Health and Global Health Perspectives. *Nat Microbiol* **2019**, *4* (9), 1432–1442. https://doi.org/10.1038/s41564-019-0503-9.

(7) Lee, J.; von Gunten, U.; Kim, J.-H. Persulfate-Based Advanced Oxidation: Critical Assessment of Opportunities and Roadblocks. *Environ Sci Technol* **2020**, *54* (6), 3064–3081. https://doi.org/10.1021/acs.est.9b07082.

(8) Zhou, T.; Du, J.; Wang, Z.; Xiao, G.; Luo, L.; Faheem, M.; Ling, H.; Bao, J. Degradation of Sulfamethoxazole by MnO2/Heat-Activated Persulfate: Kinetics, Synergistic Effect and Reaction Mechanism. *Chem Eng J Adv* **2022**, *9*, 100200. https://doi.org/10.1016/j.ceja.2021.100200.

(9) Ji, Y.; Fan, Y.; Liu, K.; Kong, D.; Lu, J. Thermo Activated Persulfate Oxidation of Antibiotic Sulfamethoxazole and Structurally Related Compounds. *Water Res* **2015**, *87*, 1–9. https://doi.org/10.1016/j.watres.2015.09.005.

(10) Zhang, B. T.; Zhang, Y.; Teng, Y.; Fan, M. Sulfate Radical and Its Application in Decontamination Technologies. *Crit Rev Environ Sci Technol* **2015**, *45* (16), 1756–1800. https://doi.org/10.1080/10643389.2014.970681.

(11) TSITONAKI, A.; PETRI, B.; CRIMI, M.; MOSBÆK, H.; SIEGRIST, R. L.; BJERG, P. L. In Situ Chemical Oxidation of Contaminated Soil and Groundwater Using Persulfate: A Review. *Crit Rev Environ Sci Technol* **2010**, *40* (1), 55–91. https://doi.org/10.1080/10643380802039303.

(12) Milh, H.; Schoenaers, B.; Stesmans, A.; Cabooter, D.; Dewil, R. Degradation of Sulfamethoxazole by Heat-Activated Persulfate Oxidation: Elucidation of the Degradation Mechanism and Influence of Process Parameters. *Chem Eng J* **2020**, *379*, 122234. https://doi.org/10.1016/j.cej.2019.122234.

(13) Yang, Y.; Lu, X.; Jiang, J.; Ma, J.; Liu, G.; Cao, Y.; Liu, W.; Li, J.; Pang, S.; Kong, X.; Luo, C. Degradation of Sulfamethoxazole by UV, UV/H2O2 and UV/Persulfate (PDS): Formation of Oxidation Products and Effect of Bicarbonate. *Water Res* **2017**, *118*, 196–207. https://doi.org/10.1016/j.watres.2017.03.054.

(14) Elsner, M.; Imfeld, G. Compound-Specific Isotope Analysis (CSIA) of Micropollutants in the Environment — Current Developments and Future Challenges. *Curr Opin Biotechnol* **2016**, *41*, 60–72. https://doi.org/10.1016/j.copbio.2016.04.014.

(15) Höhener, P.; Guers, D.; Malleret, L.; Boukaroum, O.; Martin-Laurent, F.; Masbou, J.; Payraudeau, S.; Imfeld, G. Multi-Elemental Compound-Specific Isotope Analysis of Pesticides for Source Identification and Monitoring of Degradation in Soil: A Review. *Environ Chem Lett* **2022**, *20* (6), 3927–3942. https://doi.org/10.1007/s10311-022-01489-8.

(16) Hofstetter, T. B.; Bakkour, R.; Buchner, D.; Eisenmann, H.; Fischer, A.; Gehre, M.; Haderlein, S. B.; Höhener, P.; Hunkeler, D.; Imfeld, G.; Jochmann, M. A.; Kümmel, S.; Martin, P. R.; Pati, S. G.; Schmidt, T. C.; Vogt, C.; Elsner, M. Perspectives of Compound-Specific Isotope Analysis of Organic Contaminants for Assessing Environmental Fate and Managing Chemical Pollution. *Nature Water* **2024**, *2* (1), 14–30. https://doi.org/10.1038/s44221-023-00176-4.

(17) Willach, S.; Lutze, H. V.; Eckey, K.; Löppenberg, K.; Lüling, M.; Terhalle, J.; Wolbert, J. B.; Jochmann, M. A.; Karst, U.; Schmidt, T. C. Degradation of Sulfamethoxazole Using Ozone and Chlorine Dioxide - Compound-Specific Stable Isotope Analysis, Transformation Product Analysis and Mechanistic Aspects. *Water Res* **2017**, *122*, 280–289. https://doi.org/10.1016/j.watres.2017.06.001.

(18) Birkigt, J.; Gilevska, T.; Ricken, B.; Richnow, H. H.; Vione, D.; Corvini, P. F. X.; Nijenhuis, I.; Cichocka, D. Carbon Stable Isotope Fractionation of Sulfamethoxazole during Biodegradation by Microbacterium Sp. Strain BR1 and upon Direct Photolysis. *Environ Sci Technol* **2015**, *49* (10), 6029–6036. https://doi.org/10.1021/acs.est.5b00367.

(19) Ouyang, W. Y.; Kümmel, S.; Adrian, L.; Zhu, Y. G.; Richnow, H. H. Carbon and Hydrogen Stable Isotope Fractionation of Sulfamethoxazole during Anaerobic Transformation Catalyzed by Desulfovibrio Vulgaris Hildenborough. *Chemosphere* **2023**, *311*, 136923. https://doi.org/10.1016/j.chemosphere.2022.136923.

(20) Liu, X.; Akay, C.; Köpke, J.; Kümmel, S.; Richnow, H. H.; Imfeld, G. Direct Phototransformation of Sulfamethoxazole Characterized by Four-Dimensional Element Compound Specific Isotope Analysis. *Environ Sci Technol* **2024**. https://doi.org/10.1021/acs.est.4c02666.

(21) Dou, Q.; Canavan, A.; Fu, Y.; Xiang, L.; Wang, Y.; Wang, X.; Jiang, X.; Dirr, C.; Wang, F.; Elsner, M. Nitrogen Stable Isotope Analysis of Sulfonamides by Derivatization-Gas Chromatography-Isotope Ratio Mass Spectrometry. *Anal Bioanal Chem* **2024**. https://doi.org/10.1007/s00216-024-05361-2.

(22) Maier, M. P.; Prasse, C.; Pati, S. G.; Nitsche, S.; Li, Z.; Radke, M.; Meyer, A.; Hofstetter, T. B.; Ternes, T. A.; Elsner, M. Exploring Trends of C and N Isotope Fractionation to Trace Transformation Reactions of Diclofenac in Natural and Engineered Systems. *Environ Sci Technol* **2016**, *50* (20), 10933–10942. https://doi.org/10.1021/acs.est.6b02104.

(23) Gilevska, T.; Gehre, M.; Richnow, H. H. Multidimensional Isotope Analysis of Carbon, Hydrogen and Oxygen as Tool for Identification of the Origin of Ibuprofen. *J Pharm Biomed Anal* **2015**, *115*, 410–417. https://doi.org/10.1016/j.jpba.2015.07.030.

(24) Ouyang, W. Y.; Birkigt, J.; Richnow, H. H.; Adrian, L. Anaerobic Transformation and Detoxification of Sulfamethoxazole by Sulfate-Reducing Enrichments and

Desulfovibrio Vulgaris. *Environ Sci Technol* **2021**, *55* (1), 271–282. https://doi.org/10.1021/acs.est.0c03407.

(25) Van Breukelen, B. M. Extending the Rayleigh Equation to Allow Competing Isotope Fractionating Pathways to Improve Quantification of Biodegradation. *Environ Sci Technol* **2007**, *41* (11), 4004–4010. https://doi.org/10.1021/es0628452.

(26) Elsner, M.; Zwank, L.; Hunkeler, D.; Schwarzenbach, R. P. A New Concept Linking Observable Stable Isotope Fractionation to Transformation Pathways of Organic Pollutants. *Environ Sci Technol* **2005**, *39* (18), 6896–6916. https://doi.org/10.1021/es0504587.

(27) Boreen, A. L.; Arnold, W. A.; McNeill, K. Photochemical Fate of Sulfa Drugs in Then Aquatic Environment: Sulfa Drugs Containing Five-Membered Heterocyclic Groups. *Environ Sci Technol* **2004**, *38* (14), 3933–3940. https://doi.org/10.1021/es0353053.

(28) Lee, J.; von Gunten, U.; Kim, J.-H. Persulfate-Based Advanced Oxidation: Critical Assessment of Opportunities and Roadblocks. *Environ Sci Technol* **2020**, *54* (6), 3064–3081. https://doi.org/10.1021/acs.est.9b07082.

(29) Zhao, D.; Liao, X.; Yan, X.; Huling, S. G.; Chai, T.; Tao, H. Effect and Mechanism of Persulfate Activated by Different Methods for PAHs Removal in Soil. *J Hazard Mater* **2013**, *254–255* (1), 228–235. https://doi.org/10.1016/j.jhazmat.2013.03.056.

(30) Ahmed, M. M.; Barbati, S.; Doumenq, P.; Chiron, S. Sulfate Radical Anion Oxidation of Diclofenac and Sulfamethoxazole for Water Decontamination. *Chemical Engineering Journal* **2012**, *197*, 440–447. https://doi.org/10.1016/j.cej.2012.05.040.

(31) Neta, P.; Madhavan, lb V; Haya Zemel, lb; Fessenden, R. W. Rate Constants and Mechanism of Reaction of SO4· with Aromatic Compounds. *J. Am. Chem. Soc.* **1976**, 193–167.

(32) Wojnárovits, L.; Tóth, T.; Takács, E. Rate Constants of Carbonate Radical Anion Reactions with Molecules of Environmental Interest in Aqueous Solution: A Review. *Sci Total Environ* **2020**, *717*, 137219. https://doi.org/10.1016/j.scitotenv.2020.137219.

(33) Huber, M. M.; Canonica, S.; Park, G. Y.; Von Gunten, U. Oxidation of Pharmaceuticals during Ozonation and Advanced Oxidation Processes. *Environ Sci Technol* **2003**, *37* (5), 1016–1024. https://doi.org/10.1021/es025896h.

(34) Zhang, D.; Wu, L.; Yao, J.; Herrmann, H.; Richnow, H. H. Carbon and Hydrogen Isotope Fractionation of Phthalate Esters during Degradation by Sulfate and Hydroxyl Radicals. *Chem Eng J* **2018**, *347*, 111–118. https://doi.org/10.1016/j.cej.2018.04.047.

(35) Neta, P.; Huie, R. E.; Ross, A. B. Rate Constants for Reactions of Inorganic Radicals in Aqueous Solution. *J Phys Chem Ref Data* **1988**, *17* (3), 1027–1284. https://doi.org/10.1063/1.555808.

(36) Qi, C.; Liu, X.; Lin, C.; Zhang, X.; Ma, J.; Tan, H.; Ye, W. Degradation of Sulfamethoxazole by Microwave-Activated Persulfate: Kinetics, Mechanism and Acute Toxicity. *Chem Eng J* **2014**, *249*, 6–14. https://doi.org/10.1016/j.cej.2014.03.086.

(37) Niu, J.; Zhang, L.; Li, Y.; Zhao, J.; Lv, S.; Xiao, K. Effects of Environmental Factors on Sulfamethoxazole Photodegradation under Simulated Sunlight Irradiation: Kinetics and Mechanism. *J Environ Sci (China)* **2013**, *25* (6), 1098–1106. https://doi.org/10.1016/S1001-0742(12)60167-3.

(38) Nasuhoglu, D.; Yargeau, V.; Berk, D. Photo-Removal of Sulfamethoxazole (SMX) by Photolytic and Photocatalytic Processes in a Batch Reactor under UV-C Radiation (Λmax=254nm). *J Hazard Mater* **2011**, *186* (1), 67–75. https://doi.org/10.1016/j.jhazmat.2010.10.080.

(39) Liu, R.; Yang, J. yan. Enhanced Removal of Sulfamethoxazole in Soil by Ball-Milled Fe0-FeS@BC Activated Persulfate Process. *J Environ Chem Eng* **2023**, *11* (5). https://doi.org/10.1016/j.jece.2023.110747.

(40) Wang, Y.; Zhou, C.; Wu, J.; Niu, J. Insights into the Electrochemical Degradation of Sulfamethoxazole and Its Metabolite by Ti/SnO2-Sb/Er-PbO2 Anode. *Chinese Chemical Letters* **2020**, *31* (10), 2673–2677. https://doi.org/10.1016/j.cclet.2020.03.073.

(41) Solar, S.; Solar, W.; Getoff~, N. Resolved Multisite OH-Attack on Aqueous Aniline Studied by Pulse Radiolysis. *Int. J. Radiat. Appl. Instrum* **1986**, *28* (2), 229–234.

(42) Wang, Z.; Wang, J.; Xiong, B.; Bai, F.; Wang, S.; Wan, Y.; Zhang, L.; Xie, P.; Wiesner, M. R. Application of Cobalt/Peracetic Acid to Degrade Sulfamethoxazole at Neutral Condition: Efficiency and Mechanisms. *Environ Sci Technol* **2020**, *54* (1), 464–475. https://doi.org/10.1021/acs.est.9b04528.

(43) Drouin, G.; Droz, B.; Leresche, F.; Payraudeau, S.; Masbou, J.; Imfeld, G. Direct and Indirect Photodegradation of Atrazine and: S -Metolachlor in Agriculturally Impacted Surface Water and Associated C and N Isotope Fractionation. *Environ Sci Process Impacts* **2021**, *23* (11), 1791–1802. https://doi.org/10.1039/d1em00246e.

(44) Ratti, M.; Canonica, S.; McNeill, K.; Erickson, P. R.; Bolotin, J.; Hofstetter, T. B. Isotope Fractionation Associated with the Direct Photolysis of 4-Chloroaniline. *Environ Sci Technol* **2015**, *49* (7), 4263–4273. https://doi.org/10.1021/es505784a.

(45) Ratti, M.; Canonica, S.; McNeill, K.; Bolotin, J.; Hofstetter, T. B. Isotope Fractionation Associated with the Photochemical Dechlorination of Chloroanilines. *Environ Sci Technol* **2015**, *49* (16), 9797–9806. https://doi.org/10.1021/acs.est.5b02602.

(46) Skarpeli-Liati, M.; Jiskra, M.; Turgeon, A.; Garr, A. N.; Arnold, W. A.; Cramer, C. J.; Schwarzenbach, R. P.; Hofstetter, T. B. Using Nitrogen Isotope Fractionation to Assess the Oxidation of Substituted Anilines by Manganese Oxide. *Environ Sci Technol* **2011**, *45* (13), 5596–5604. https://doi.org/10.1021/es200743t.

661

662 **TOC**

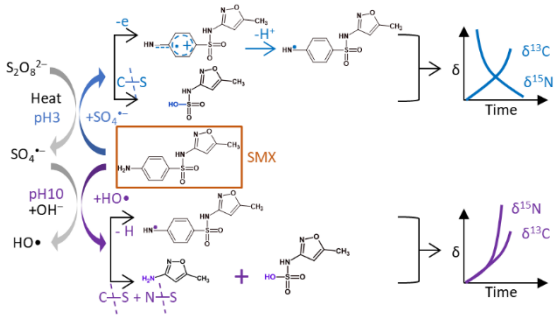

663

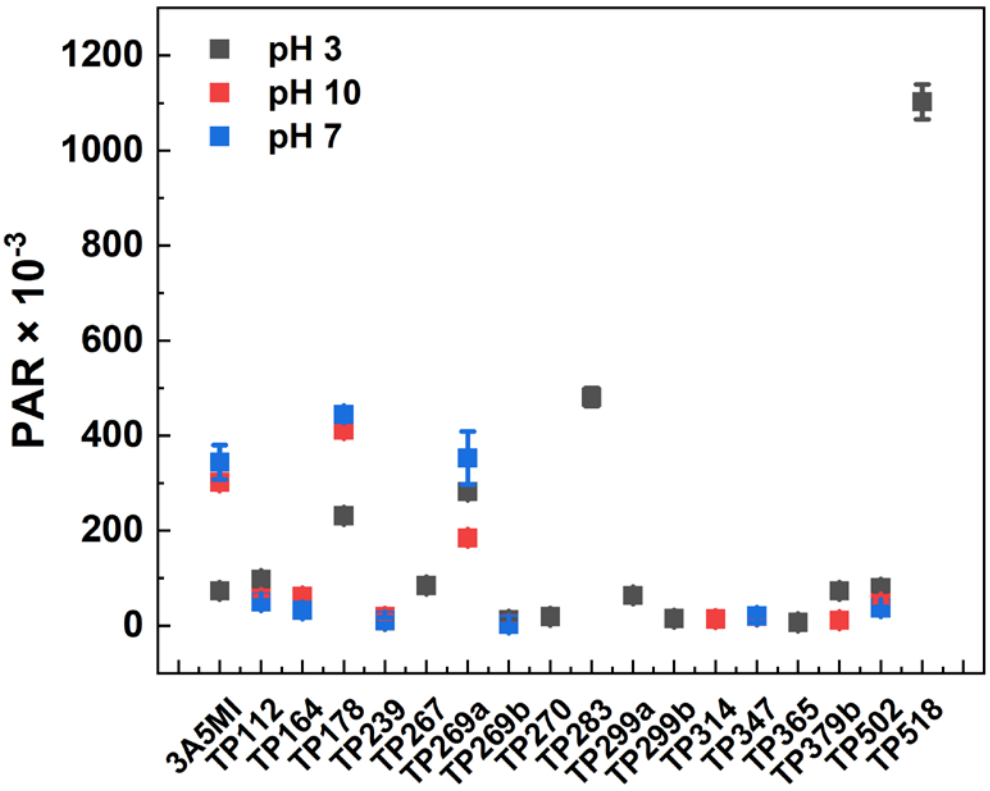

664

665 **Figure 1.** Formation patterns of the TPs during SMX phototransformation at pH 3, 7 and 10.
666 TPs are represented as peak area ratios (PAR), defined as the ratio of the transformation product
667 peak area to the peak area of initial SMX at each pH level. The results are based on the
668 maximum PAR during the reaction.

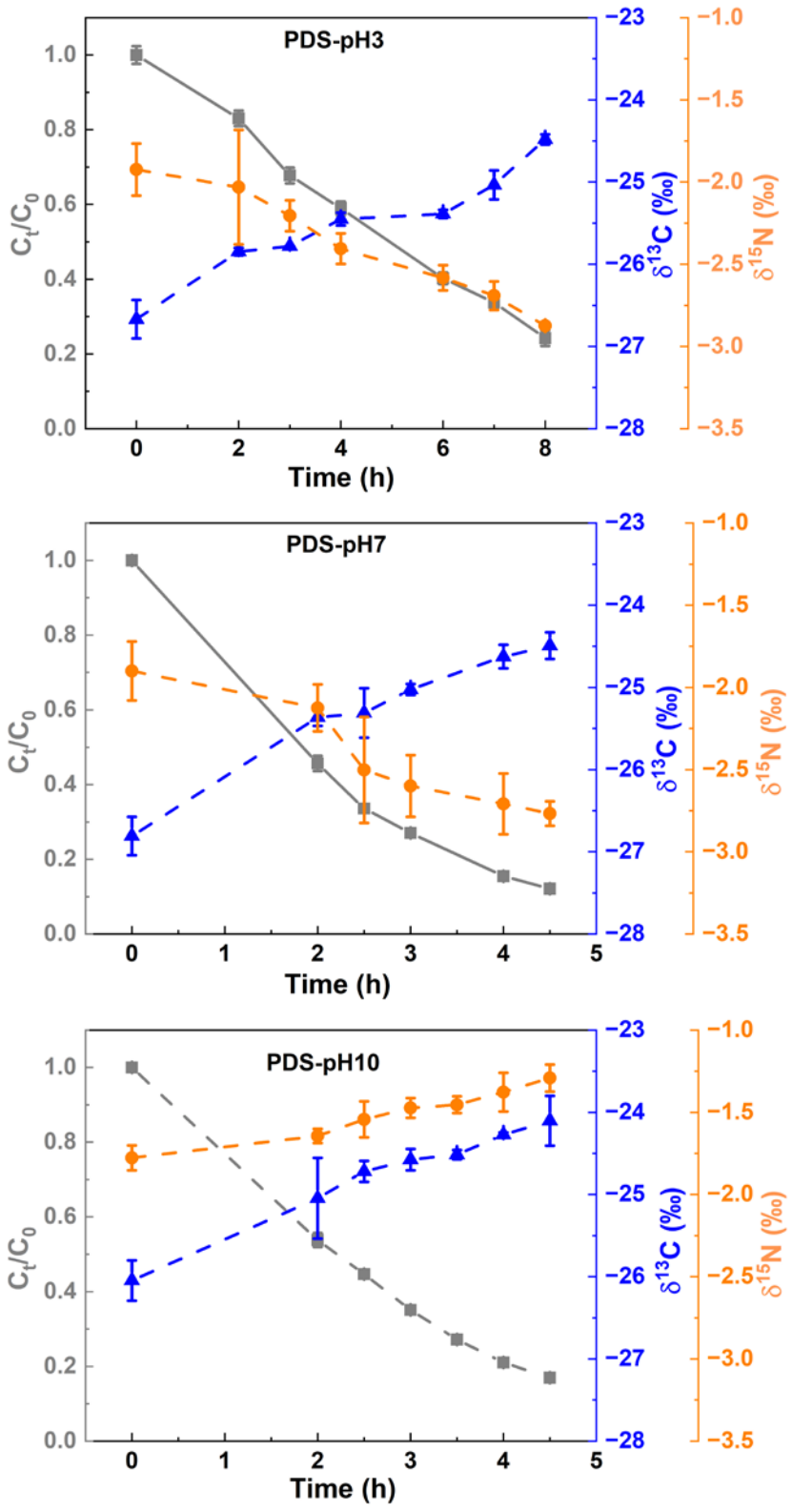

669

670 **Figure 2.** Carbon and nitrogen isotope fractionation during PS transformation of SMX at pH 3,

671 7 and 10. The error bars represent the standard error of triplicate measurements.

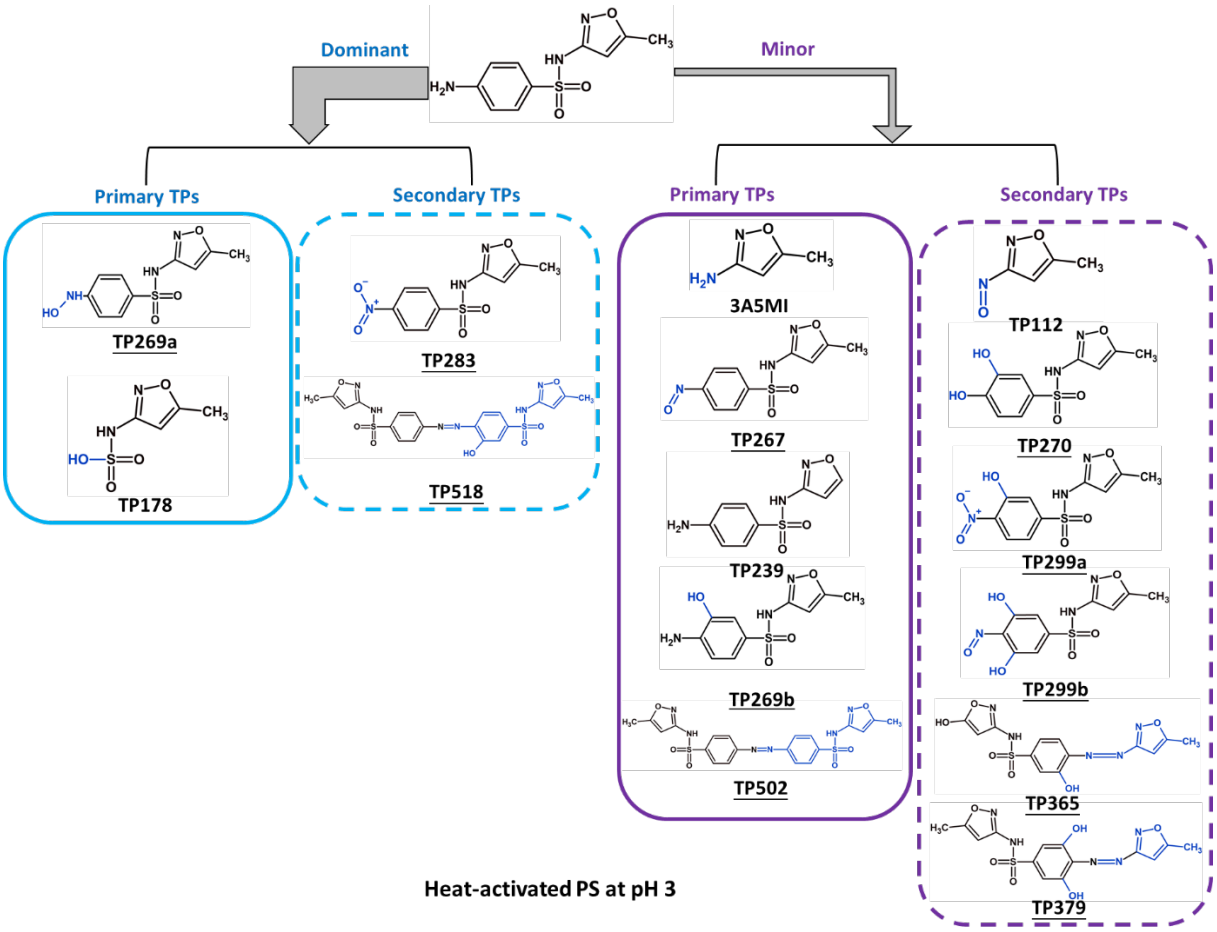

672

673 **Scheme 1.** Proposed transformation pathways of SMX by PS at pH 3. The dominant and minor
674 TPs are classified based on the PAR values. Primary TPs are defined as those that originate
675 directly from the parent compound (SMX), while secondary TPs are those derived from primary
676 TPs. The TPs underlined in the schemes indicate those with a mass greater than that of SMX,
677 which is 253.

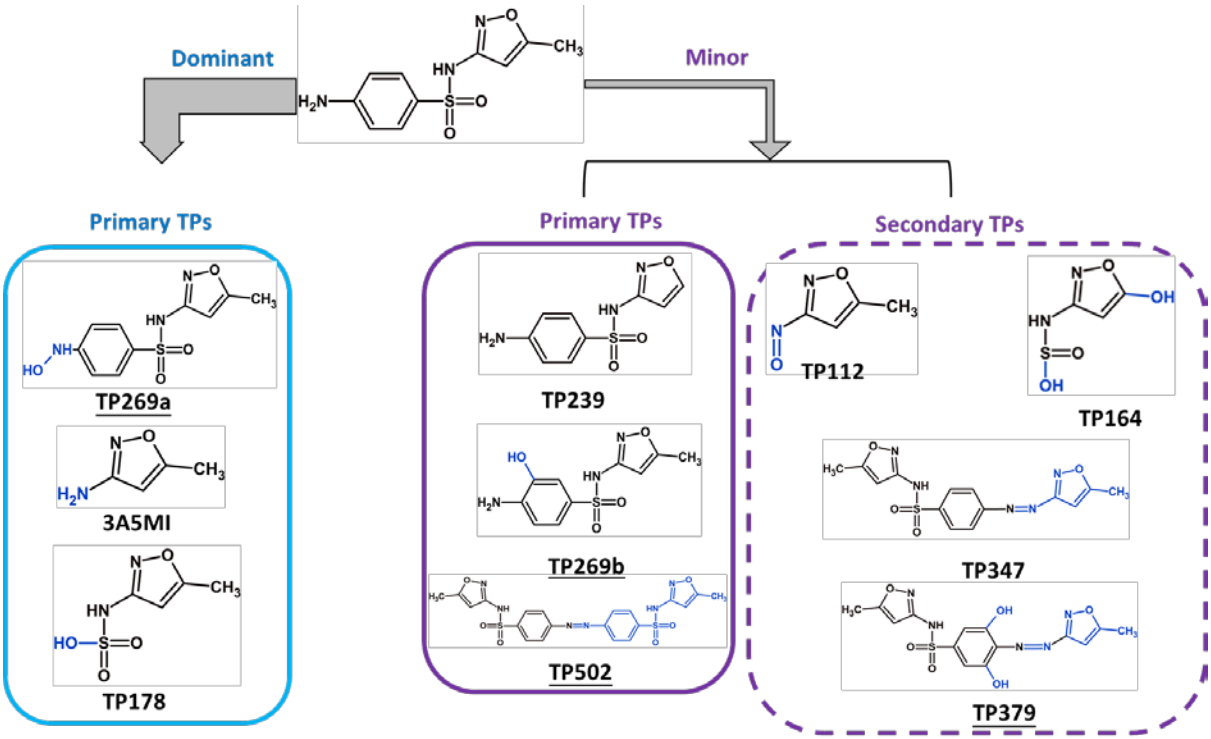

678

679 **Scheme 2.** Proposed transformation pathways of SMX by PS at pH 10. The dominant and minor
680 TPs are classified based on the PAR values. Primary TPs are defined as those that originate
681 directly from the parent compound (SMX), while secondary TPs are those derived from primary
682 TPs. The TPs underlined in the schemes indicate those with a mass greater than that of SMX,
683 which is 253.

684

685

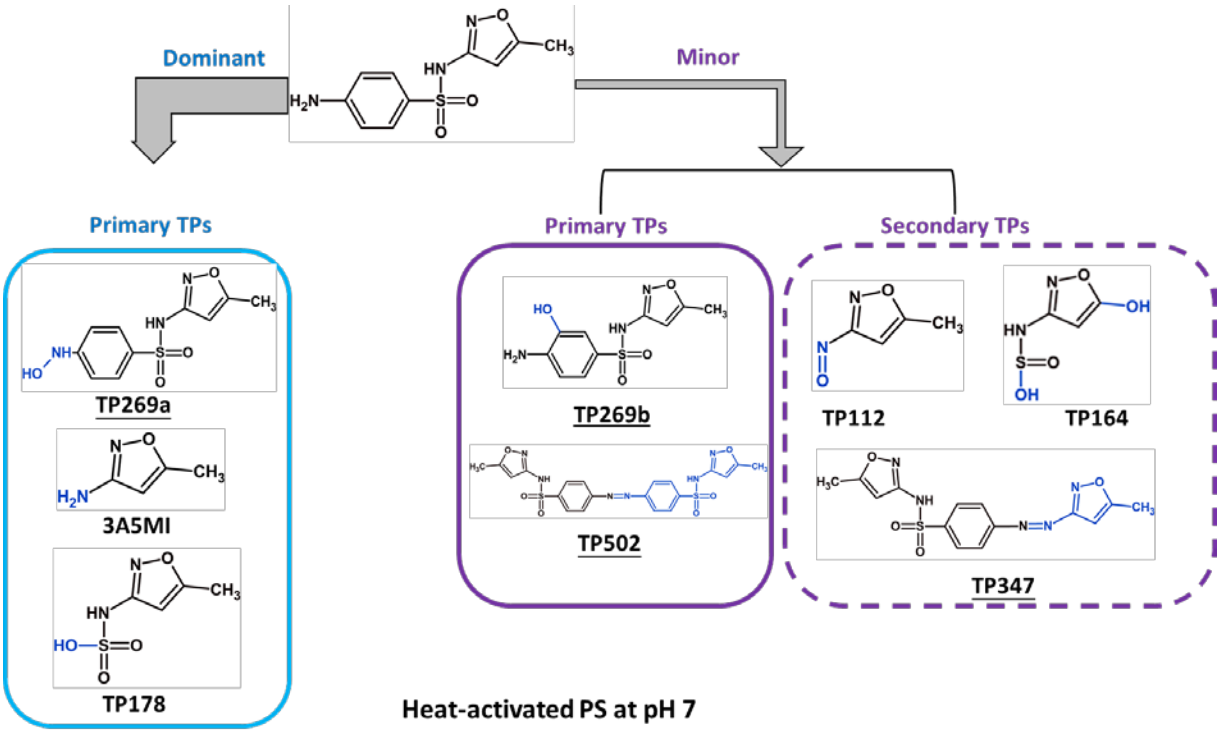

686

687 **Scheme 3.** Proposed transformation pathways of SMX by PS at pH 7. The dominant and minor
688 TPs are classified based on the PAR values. Primary TPs are defined as those that originate
689 directly from the parent compound (SMX), while secondary TPs are those derived from primary
690 TPs. The TPs underlined in the schemes indicate those with a mass greater than that of SMX,
691 which is 253.

692

693

694

695

Table 1. Kinetics, carbon and nitrogen isotopic fractionation (ε_C and ε_N), apparent ^{13}C and ^{15}N-Kinetic Isotope Effects (^{13}C-AKIE and ^{15}N-AKIE), and dual element isotope values ($\Lambda_{N/C}$) with 95% confidential interval associated with SMX heat-activated PS transformation. Available ε_C, ε_N and ^{13}C-AKIE values with 95% confidential interval of SMX in phototransformation, biotransformation and other radical oxidation from literature.

Reactions		pH	Kinetics (h^{-1})	ε_C (‰)	ε_N (‰)	^{13}C-AKIE	^{15}N-AKIE	$\Lambda_{N/C}$	
Heat-activated PS	Single electron transfer + bond cleavage	3	0.1786±0.0218	−1.3±0.5	+0.68±0.11	1.013±0.005	0.998±0.001	−0.5±0.2	this study
	Single electron transfer + H abstraction + bond cleavage	7	0.4775±0.0480	−1.1±0.4	+0.44±0.18	1.011±0.004	n.d.	−0.4±0.2	
	H abstraction + bond cleavage	10	0.4001±0.0605	−1.1±0.3	−0.27±0.04	1.011±0.004	n.d.	+0.2±0.1	
Direct phototransformation	Multi-bond cleavages	3		−2.8±0.4	+3.6±0.1	1.014±0.002		−1.3 ± 0.2	Liu et al., 2024[20]
		7		−2.0±0.2	+3.0±0.2			−1.5 ± 0.2	Liu et al., 2024[20]
Aerobic biotransformation (*Microbacterium* sp. strain BR1)	Ipsohydroxylation			−0.6±0.1		1.006±0.001			Birkigt et al., 2005[18]

Anaerobic biotransformation (*Desulfovibrio vulgaris* Hildenborough,)	Reductive N-O bond cleavage		−5.8±0.7	1.029±0.003	Ouyang et al., 2023[19]
O_3 Oxidation		3	−1.2±0.1		Willach et al., 2017[17]
ClO_2 Oxidation	Hydroxylation	3	−0.8±0.1		Willach et al., 2017[17]
ClO_2 Oxidation		8	−1.3±0.1		Willach et al., 2017[17]

n.d. represents not determined.